A Microphysiological System for Studying Barrier Health of Live Tissues in Real Time

Thomas Chen

Thomas.chen@colostate.edu

Colorado State University

Ryan Way
Colorado State University

Hayley Templeton
Colorado State University

Daniel Ball
Colorado State University

Ming-Hao Cheng
Colorado State University

Stuart Tobet
Colorado State University

Additional Declarations: There is **NO** Competing Interest.

A Microphysiological System for Studying Barrier Health of Live Tissues in Real Time

Ryan Way[1], Hayley Templeton[2], Daniel Ball[1], Ming-Hao Cheng[1], Stuart A. Tobet[2,3], Thomas Chen[1,3*]

[1]Department of Electrical & Computer Engineering, Colorado State University, Fort Collins, CO, USA.
[2]Department of Biomedical Sciences, Colorado State University, Fort Collins, CO, USA.
[3]School of Biomedical Engineering, Colorado State University, Fort Collins, Colorado, USA

Abstract

Epithelial cells create barriers that protect many different components in the body from their external environment. The gut in particular carries bacteria and other infectious agents. A healthy gut epithelial barrier prevents unwanted substances from accessing the underlying lamina propria while maintaining the ability to digest and absorb nutrients. Increased gut barrier permeability, better known as *leaky gut*, has been linked to several chronic inflammatory diseases. Yet understanding the cause of leaky gut and developing effective interventions are still elusive due to the lack of tools to maintain tissue's physiological environment while elucidating cellular functions under various stimuli ex vivo. This paper presents a microphysiological system capable of recording real-time barrier permeability of mouse gut tissues in a realistic physiological environment over extended durations. Key components of the microphysiological system include a microfluidic chamber designed to hold the live tissue explant and create a sufficient microphysiological environment to maintain tissue viability; proper media composition that preserves a microbiome and creates necessary oxygen gradients across the barrier; integrated sensor electrodes and supporting electronics for acquiring and calculating transepithelial electrical resistance (TEER); and a scalable system architecture to allow multiple chambers running in parallel for increased throughput. The experimental results demonstrate that the system can maintain tissue viability for up to 72 hours. The results also show that the custom-built and integrated TEER sensors are sufficiently sensitive to distinguish differing levels of barrier permeability when treated with collagenase and low pH media compared to control. Permeability variations in tissue explants from different positions in the intestinal tract were also investigated using TEER revealing their disparities in permeability. Finally, the results also quantitatively determine the effect of the muscle layer on total epithelial resistance.

1 Introduction

Epithelial cells are the body's first line of defense for protecting a mammalian host from its external environment[1]. The reliability of these barriers is important in the body's continued health and homeostasis[1–3]. This makes the health and any chemical response of epithelial cells, specifically in the gut, an important field of study for researchers. Therefore, many devices and methods have been created and investigated to study the epithelial cell layers as they would be in the body. One of the first devices was the Ussing Chamber, named after the Danish biologist Hans Ussing[4]. The Ussing chamber was originally designed to understand the phenomenon of active NaCl transport across frog skin[4,5]. This technique set the groundwork and created the first model for epithelial ion transport. More modern designs of Ussing systems have been made to accommodate many different types of epithelial barriers found inside an animal. These barriers include skin, intestinal, esophageal, and more[3,5–8]. There are several common issues with current Ussing chamber designs. They include the use of expensive benchtop equipment; static media within the chamber;

low throughput; and bulky experimental setup. Despite these shortcomings the Ussing chamber is one of the most used tools for ex-vivo measurements of epithelial permeability, through paracellular flux or electrical measurements.

Transepithelial/transendothelial electrical resistance (TEER) is a widely accepted measure of the integrity of cellular barriers[3]. To quantify the integrity of tight junctions in an epithelial barrier, many researchers have performed experiments to determine the TEER of the barrier. Junction integrity of epithelial barriers can also be evaluated by using fluorescently labelled probes to visualize the paracellular flux across the epithelium[9–14]. Most of the studies using TEER to measure the integrity of tight junctions in epithelial barriers use in-vitro cell culture models of endothelial and epithelial monolayers in a Transwell system[12,15–17]. More recently, organ-on-a-chip (OoC) devices have been proposed. These are more advanced devices which often incorporate microfluidics for maintaining cell culture[12,18–20]. These devices are made to resemble in vivo environments more accurately, both biochemically and physically[10,21]. One of the most important features in these devices to recreate the body's physiology is the built-in microfluidics to simulate fluid flow and shear stress on the epithelial barrier[10]. OoC devices also provide the opportunity to have built-in electrodes for electrical measurement of barrier integrity. While the results from the experiments using both Transwell and OoC devices have enhanced our understanding of the transepithelial transport process, their capabilities are limited by using an in-vitro cell culture to model the epithelial barrier which cannot replicate the full complexity of the epithelial barrier in live tissues[13].

Live tissue in an ex vivo environment provides a much more realistic physiological model. Ex vivo epithelial/endothelial models can include the full variety of cells throughout the barrier, this is something that cannot be replicated in cells grown in culture experiments. Along with the advantages of working with ex vivo tissue also comes several difficulties. These difficulties include tissue dissection/preparation, tissue viability, sterilization, and added diffusion layer resistance[22]. It is also more difficult to maintain viability of live tissues for an extended period of time. With reduced tissue viability, experiments using live tissues in an Ussing chamber have often been limited to under 3 hours[5,22]. This is often not sufficiently long enough for the tissue to be settled into its new environment inside the chamber, or to conduct experiments with live tissue. To develop more physiologically realistic ex vivo models it is important to increase tissue viability to allow experiments to be conducted for a longer period. This can be achieved through the addition of microfluidics and appropriate media composition in the device[11,13]. Microfluidics create a more accurate physical environment for the live tissue explant (e.g., fluid flow and shear stress) and the media composition provides the tissue with appropriate nutrient diffusion[13].

This paper presents a microphysiological system for ex vivo tissues with integrated sensors and electronics. Our contribution is threefold: first, the microphysiological system is capable of keeping tissue explants viable for up to 72 h; second, the TEER measurement of the ex vivo tissue is supported by integrated electrodes and the highly integrated backend electronics to record real-time TEER measurements throughout the entirety of the experiment at a user-specified interval, thus, allowing users to observe the evolution of barrier integrity in real time; third, the system architecture is fully scalable allowing multiple microfluidic chambers to be connected to the microphysiological system at a time to increase throughput, and more importantly, to allow controlled experiments using live tissues from the same donor at the same time. All these features are crucial attributes to biomedical research and drug discovery.

2 Methods

Microfluidic Chamber Design

The microfluidic chamber (Fig. 1a-e), to be referred to as *chamber* for short, was designed using CAD (Autodesk, Inc) and fabricated using Anycubics UV sensitive resin and SLA printer. To avoid harmful effects from uncured resin, each chamber is fully cured using UV light and thoroughly rinsed with isopropyl alcohol. It is further sterilized in a low-temperature autoclave. The chamber consists of two halves assembled to hold the tissue and make connections to the integrated TEER electrodes. Each half chamber

is composed of the following (Fig. 1a): the chamber body; two 1mm thick PDMS layers for holding the electrode chip in place; one gold electrode chip; an aluminum clamp; and a printed circuit board (PCB) with spring headers that connect to the electrode chip. The fully assembled chamber (Fig. 1b) consists of two halves, the top half has spikes to hold the tissue tight when the chamber is sealed; the bottom half has corresponding openings for these spikes and is where the tissue is placed before closing the chamber. Fig. 1c shows how the tissue explant positioned on the bottom half chamber, before and after the experiment. When the tissue is enclosed in the device, the chamber spikes puncture around the outer edge of the tissue but leaves the center untouched. A PDMS layer is placed over the spikes of the top chamber to create a flush seal against the tissue and to prevent any leaks between the chamber halves after the chamber is closed. A fully assembled chamber is shown in Fig. 1d and e in the front and the back view of the device, respectively.

Tubing is connected to each chamber half through Luer lock connectors. Media is pumped into the chamber using custom-designed syringe pumps where users can specify start and stop time points throughout the experiment period. With the tissue positioned over the circular opening between the chamber halves, a barrier is formed between the two media flows, one for the serosal side and the other for the luminal side of the tissue. The microfluidic path flows over the opening on each side exposing the tissue to the media composition. Providing balanced flow for the tissue inside the chamber is important for controlling shear stress and extending tissue viability[10,13,20]. The chamber was designed using 3D fluid simulations (CFD, Autodesk Inc) to make the media flow over the tissue area with uniform velocity as possible. Fig. 1f shows an example of the flow simulations performed during design.

Each chamber half has its own PCB breakout board that connects to the glass chip electrodes through gold spring headers. The spring headers are compressed against the chip during assembly. The PCB on the top half chamber has external wire connectors for connecting to the bottom halve PCB. The bottom PCB includes a card edge connector that is plugged into the top of the enclosure for the microphysiological system (see Section System Overview below). The chamber, when plugged into the system, is oriented vertically, making the media flow in from the bottom and out above the tissue (Fig. 1f). This orientation helps push air bubbles to the top and get them pushed out of the media outlet during experiments. Air bubbles can injure the tissue and cause large deviations for the TEER measurement.

System Overview

The entire electronic support system is housed in a metal enclosure (Figs. 1g and h) to shield all electronics from the external physical environment as well as EMF noise. USB ports provide user configuration and control of the experiment from the host computer. The connectors on the microfluidic chambers and the system enclosure are all universal, allowing for plug-and-play functionality. The current implementation can hold up to three chambers at a time (Figs. 1g and h). The entire system has a footprint of a typical laptop computer designed to allow it to fit into a limited environment chamber space during experiments. The supporting electronics are responsible for signal acquisition, signal conditioning and amplification, analog to digital conversion, and communication with the host computer via the USB protocol. A custom-built graphic user interface (GUI) was designed to allow user configurations and real-time control for the experiment. The TEER measurement data are acquired by the host computer and TEER results are calculated and displayed in the GUI.
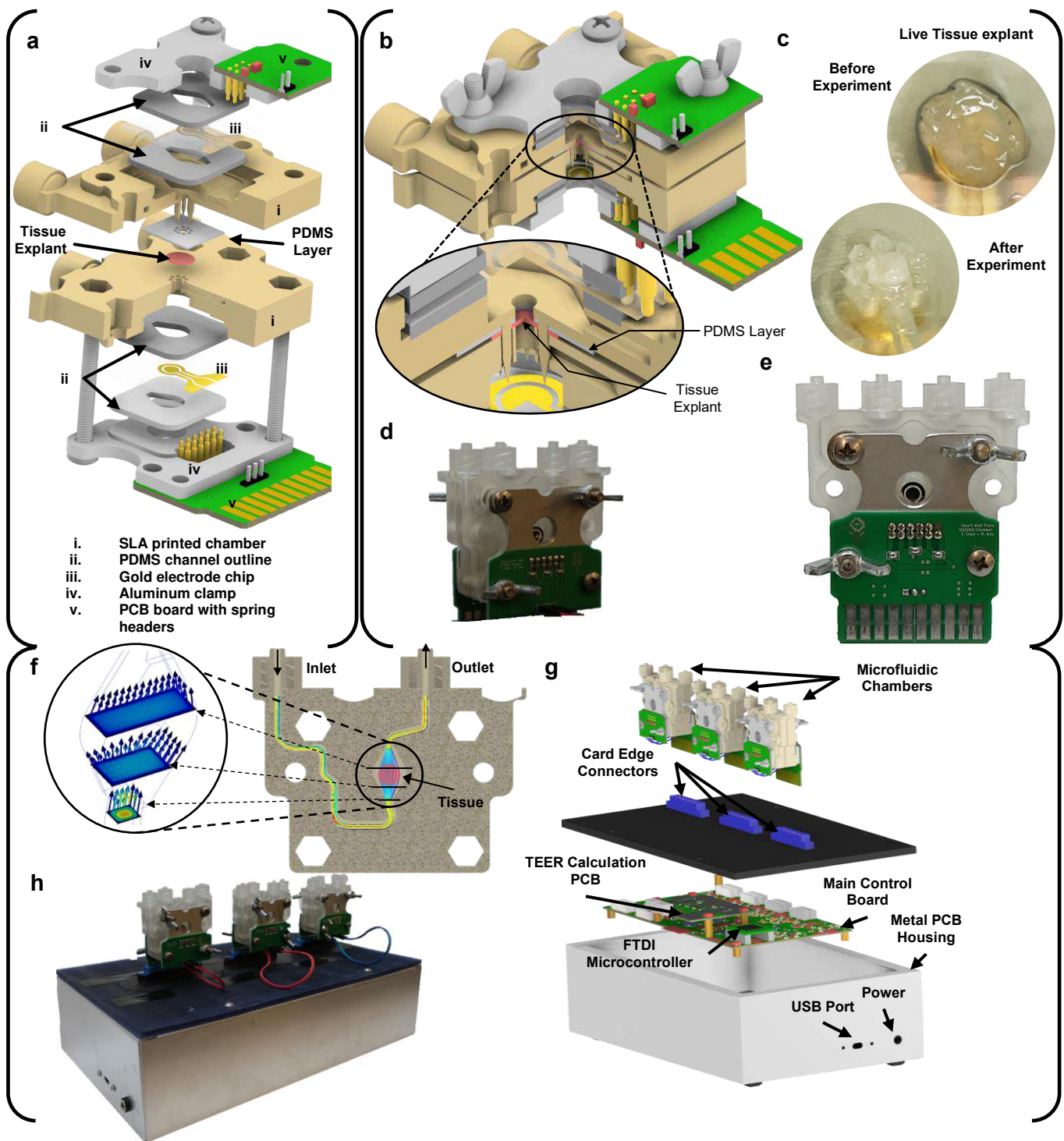
Figure 1: **Major components of the microphysiological system**. Including the microfluidic chamber **(a-f)** and the system-level housing **(g-h)**. **a)** Expanded view of a full chamber, with all components labelled. **b)** Closed chamber with a closeup view of the tissue and PDMS clamped between two chamber halves. **c)** Tissue explant before and after the experiment. **d)** and **e)** The actual manufactured chamber assembled (front and back, respectively). **f)** Flow simulation through the chamber's microfluidics. **g)** Expanded view of the microphysiological system. **h)** The actual manufactured and fully assembled system with three chambers connected the system.

Labels within figure:

i. SLA printed chamber
ii. PDMS channel outline
iii. Gold electrode chip
iv. Aluminum clamp
v. PCB board with spring headers

Tissue Explant · PDMS Layer · Live Tissue explant · Before Experiment · After Experiment · Inlet · Outlet · Tissue · Microfluidic Chambers · Card Edge Connectors · TEER Calculation PCB · Main Control Board · Metal PCB Housing · FTDI Microcontroller · USB Port · Power

Electronic Circuits for TEER Measurement

The block diagram of the electronic circuits to perform TEER measurement is shown in Fig. 2a. The TEER measurement is operated in the constant-current mode to avoid accidental over-current to damage electrodes and tissues inside the chamber. An FTDI module is used to provide interface between the host computer and the on-board electronics using the USB protocol. This interface allows users to control all internal enable signals from the GUI. A signal generator is used to generate a user defined AC voltage signal. This voltage signal is used to control a Howland current source (HCS), creating an AC current stimulus signal to the TEER electrodes. The HCS (Fig. 2b) is chosen because it can easily achieve high output impedance, signal to noise ratio (SNR), and is fully programmable through external control voltages[23,24]. Up to three parallel current stimulation signals are used for the three independent chambers in the system. The read-channel (Fig. 2b) consists of a transimpedance amplifier to convert the input current signal to an output voltage, and an instrumentation amplifier to acquire the voltage response from the tissue barrier. A relay is placed in parallel with each microfluidic chamber to discharge built-up charge on the TEER electrodes when necessary. Built-up charge on the electrodes is capable of altering the DC voltage at the input to the microfluidic chamber, and therefore, has a large enough effect to shift the DC voltage towards supply rails, reducing the dynamic range of TEER measurement.

The HCS (Fig. 2b) uses an ultra-low offset voltage operation amplifier and consists of five high precision film resistors and a single feedback capacitor for bandwidth control. High output impedance is achieved by resistor matching. The response TEER voltage from the chamber is read by an instrumentation amplifier (INA) with low input bias current. The INA gain is controlled by the resistor R_g. The response TEER current from the chamber is read using a transimpedance amplifier (TIA), with the current gain set by R_{gain}. An analog-to-digital converter (ADC) is used to convert the amplified analog outputs from the read-channel to a digital signal that is sent to the host computer via the USB port. Due to different operating voltages of different components along the signal chain to achieve the required output dynamic range, electronic level shifting is required at various points in the system. They are performed by operational amplifiers where the voltage gain is controlled by on board resistors and DC shift is adjusted using a digital potentiometer. The digital potentiometer is calibrated before each measurement using a binary search algorithm to find the smallest DC offset current. The input stimulus was also designed to have a high and low current setting to maximize the system's output dynamic range.

The supporting electronics are partitioned into two separate PCB boards. The main control board (Fig. 2e) contains the external power supply, USB connectors, microcontroller, ADC, signal generators, level shifters for control signals, and connectors to the TEER acquisition board. The TEER acquisition board (Fig. 2d) contains the HCSs, the read channels for each chamber, the calibration digital potentiometers, and the connections for the card edge connectors. Even though the system allows three chambers to be used at a time, the system architecture was designed to be scalable to allow future expansion to accommodate more chambers and sensors.

Electrode Design and Manufacturing

The electrodes are manufactured in gold on a glass substrate. Each electrode chip consists of two gold (Au) electrodes to allow 4-point measurement. The electrode chip (Fig. 2c) was fabricated on a 25mm x 25mm glass substrate through an in-house photolithography, deposition, and lift-off process. The mask was designed using AutoCAD software (Autodesk, Inc.) and manufactured by Artnet Pro (San Jose, CA). The full photolithography steps are described previously[25].
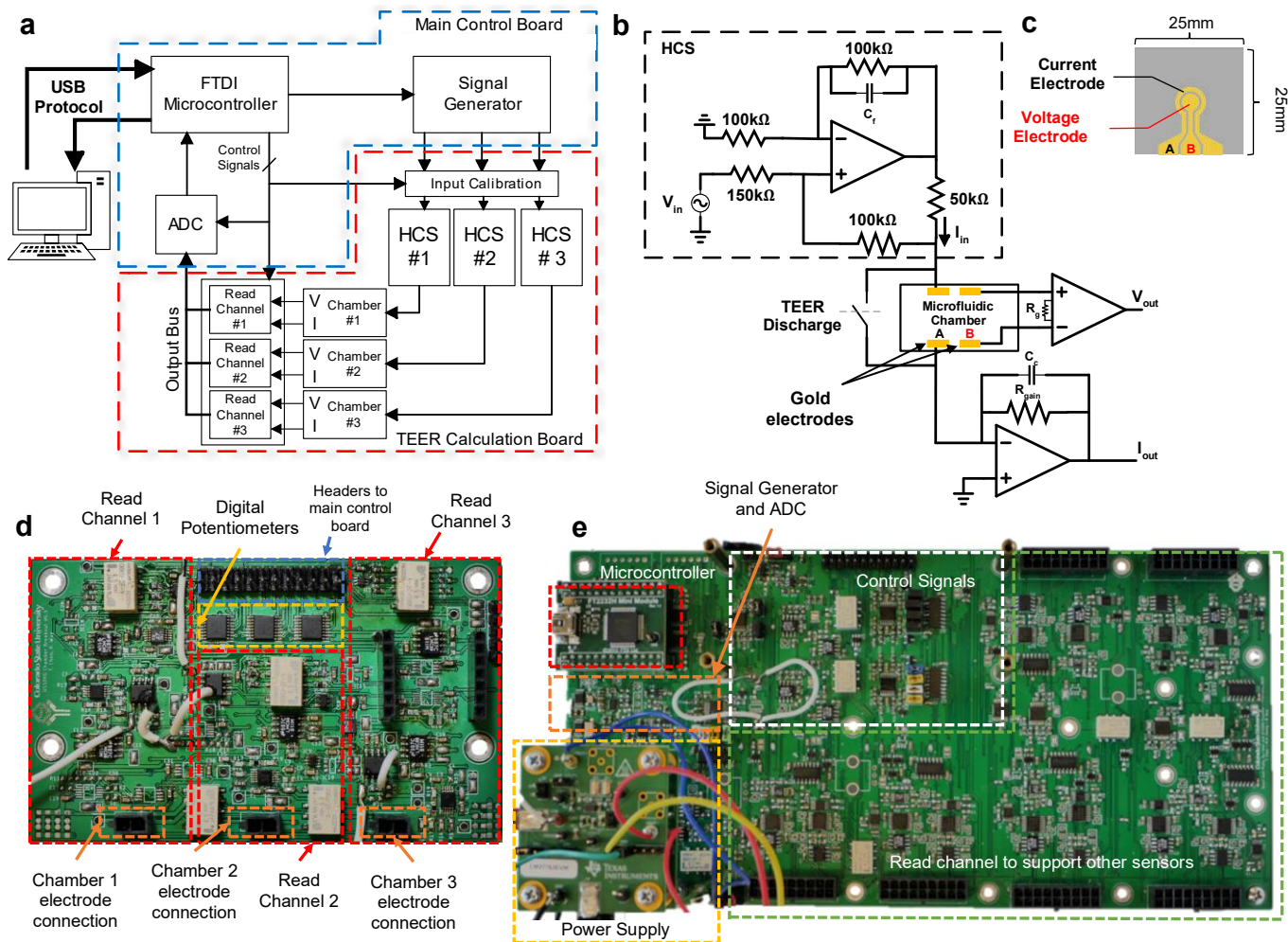
Figure 2: Microphysiological system's supporting electronics a) Block diagram showing the flow of signal conditioning and processing. **b)** Read channel circuit, responsible for supplying stimulus signal and reading output voltage and current signals directly from the sensor electrodes inside the chamber. **c)** The sensor electrodes on glass substrate, outer ring electrode is the current electrode, and the middle circle is the voltage electrode. **d)** TEER acquisition board contains all read channels, digital potentiometers, connectors for the electrodes, and connectors to the main control board. **e)** Main control board which has the power supply, signal generator and ADC, microcontroller, and control signals.

Chamber Sterilization

To prevent infection during experiments, all components of the microfluidic chamber (chamber body, glass electrode chip, PDMS layers, PCBs, tubing, and Luer locks) were put through the first round of sterilization protocol:

1. 20-minute bath in 1:10 bleach to water ratio.
2. 10-minute soapy water bath inside of ultrasonic cleaner.
3. Next, thoroughly rinse with DI water.
4. 45-minute bath in 70% ethanol.
5. Finally, thoroughly rinse with DI water and let air dry.

After the first round of sterilization, the chamber was fully assembled with metal screws and clamps that have been autoclaved (30-minute, gravity cycle). After all chambers are assembled, the chambers went through low temp gas sterilization and are kept in a sealed bag before use.

Animals, Tissue Collection, and Media Preparation

In all experiments, male C57BL/6 background mice aged 3-4 months were used. Mice were kept on a 12-h light/dark cycle with access to standard chow and water ad libitum. Animal protocols were approved by the Institutional Animal Care and Use Committee (IACUC) at Colorado State University under United States Department of Agriculture (USDA) guidelines.

Mice were deeply anesthetized with isoflurane and terminated via decapitation to prepare for tissue collection. The intestines were removed and immediately placed in 4°C 1x Krebs buffer (in mM: 2.5 KCl, 2.5 $CaCl_2$, 126 NaCl, 1.2 $MgCl_2$, 1.2 NaH_2PO_4). To prevent contractions during dissection, the Krebs buffer contained 1µl/1mL1mM nicardipine (Sigma Aldrich, St. Louis, MO), an L-type calcium ion channel blocker. Colon was then dissected to remove any remaining mesentery. For experiments in which muscle was removed, a 26G needle was used to gently tease away the muscle layer on the mesenteric edge of the tissue. Tissue was then cut longitudinally using angled vascular scissors to form flat pieces of tissue around ~5 mm.

Adult Neurobasal media was custom made in house with 2% B27 supplement (Thermo Fisher scientific, Waltham, WA), 4 mM glucose, 3% 1 M HEPES buffer (Sigma Aldrich, St. Louis, MO), without phenol red. To help maintain the gut microbiome, luminal media contained 0.4 mg/ml inulin (soluble fiber) and 0.5 M sodium sulfite (oxygen scavenger) to decrease oxygen levels[17]. The serosal media had ambient levels of oxygen creating an oxygen gradient across the tissue which we previously demonstrated[14] is necessary for preservation of a physiologically relevant bacterial community. After 24 h, luminal media for control tissue was not changed. Treatment group luminal media contained 5.80*10-2 U of broad spectrum bacterially sourced collagenase (Worthington Biochemical, Lakewood, NJ) or was treated with hydrochloric acid (HCl) to acidify the pH to 2. After completion of experiments, 0.05 M phosphate buffered saline (PBS) containing 0.5% cetylpyridinium chloride (CPC) was gently pipetted onto the tissue to preserve the mucus layer. The tissue was then gently removed from the device and placed in 4% paraformaldehyde (PFA) containing 0.5% CPC at 4°C for 24 h. Tissue was stored in PBS at 4°C until sectioning.

Tissue Sectioning and Histochemistry

Detailed methodology can be found in our previous publication[11]. Briefly, 1-3 mm sections of colon were submerged in agarose until polymerization. Tissue was then cut on a vibrating microtome (VT100S; Leica microsystems, Wetzlar, Germany) at a thickness of 50 µm. For lectin and immunohistochemistry, sections were first washed in 1x PBS, then incubated in 0.1M glycine followed by PBS washes and incubated in 0.5% sodium borohydride followed by PBS washes. Sections were then blocked in PBS with 5% normal goat serum (NGS; Lampire Biological, Pipersville, PA), 1% hydrogen peroxide, and 0.3% Triton X (TX). Next, sections were placed in PBS containing 0.3% TX and 5% NGS with the appropriate lectin or antibody for 2 days. The lectin used was Ulex Europaeus Agglutinin I conjugated to Rhodamine (UEA-1; Vector Labs) at a concentration of 0.125 µg/mL. Primary antibodies used were anti-claudin1 (Invitrogen) 1:200 and anti-peripherin (Sigma-Aldrich) 1:300. After lectin or primary antibody incubation, sections were washed in PBS with 1% NGS. Sections incubated in primary antibody were then incubated with PBS containing 0.02% TX and Alexa Fluor 594 conjugated to secondary antibodies specific to the species of the primary antibodies at a 1:500 dilution. Finally, sections were washed in PBS, mounted on slides, and cover slipped. Images were taken using a Zeiss LSM800 upright confocal laser scanning microscope and a 20x (W Plan-Apochromat 20X/1.0 DIC Vis-ir ∞ /0.17) objective or an Olympus BH2 brightfield microscope.

TEER Calculation

Processing of TEER signals involves conditioning steps to reduce noise and other artifacts. The conditioned signals were further processed by applying a curve fitting algorithm to obtain the magnitude and phase of the voltage and current response signals. The impedance magnitude ($|Z|$) and phase difference

(θ_{diff}) can then be calculated using Eqs. (1) and (2). Where Av_{current} and Av_{voltage} are the current and voltage gain values and θ_{current}(deg) and θ_{voltage}(deg) are the current and voltage respective phase values.

$$|Z| = \frac{V_{\text{peak}}}{I_{\text{peak}}} * \frac{Av_{\text{current}}}{Av_{\text{voltage}}} \quad (1)$$

$$\theta_{\text{diff}} = \theta_{\text{voltage}}(\text{deg}) - \theta_{\text{current}}(\text{deg}) \quad (2)$$

The magnitude and phase values are determined for each frequency to obtain the impedance spectrum of the tissue sample, commonly referred to as *electrical impedance spectroscopy* (EIS). Due to its versatility of revealing impedance information across a wide range of frequencies, EIS is a widely-used technique to discover the impedance characteristics of tissue/cell-culture samples in Ussing Chambers, Organ-on-a-chip devices, and well inserts[8,12,19,20,23,26–31].

The sinusoidal curve fitting is necessary to further reduce noise and unwanted artifacts in the acquired TEER signal as it is illustrated in Figs. 3a-c. The smoothed signal can provide more accurate magnitude and phase values for the subsequent TEER calculation (Fig. 3c). The curve fitting algorithm also provides drifting correction to the acquired voltage response signal. Drifting of the response voltage signal is caused by offset DC current from the Howland circuit. This offset DC current builds up charge on the serial capacitance associated with electrode's double layer capacitor, resulting in a constant rate increasing (or decreasing) of the DC voltage at the voltage electrodes from the chamber. This effect can be seen in Fig. 3a. The time dependent DC shift of the sinusoidal signal in Fig. 3a needs to be leveled before the sinusoidal curve fitting algorithm can be applied to obtain its magnitude and phase. This is done by subtracting a 1st-order polynomial function from the acquired (drifted) voltage signal as illustrated in Fig. 3b.

The TEER value of an epithelial barrier is the resistance of the transcellular and paracellular pathways combined. However, the TEER values obtained from Eqs. (1) and (2) include additional impedance such as the electrode double-layer capacitance and the media bulk resistance[3,9,30]. In order to obtain the actual TEER values associated with the epithelial barrier, baseline TEER measurements were performed for each experiment to capture the medial bulk resistance. The final TEER value of interest was obtained by subtracting the baseline TEER values from the acquired TEER values. It should be noted that the magnitude $|Z|$ used for TEER measurements should be at an appropriate frequency not too low where the impedance of the electrode double-layer capacitance dominates, and also not too high where the epithelial layer is shorted by its parallel capacitance, this can be deduced from the equivalent circuit of the epithelial barrier[9]. From the impedance spectrum of the tissue measured with this device, it was found that this value is close to 5kHz.

The TEER value can also be calculated by finding the DC response from a square wave. Since the microfluidic chamber system is also capable of producing a square wave stimulus signal, the TEER using the square waveform stimulus was also calculated. This value shows the pure resistance of the tissue barrier. Figs. 3d-e shows a set of TEER values obtained using a 5kHz sinusoidal stimulus vs. a square wave stimulus. It was found that the TEER values obtained using the square waveform are lower (7.2% on average, n = 10) than those obtained using the 5kHz sinusoidal waveform by a constant margin. This is due to the fact that the relatively fast transitions in the square waveform stimulus were able to significantly reduce the effect of the double layer capacitance associated with the electrodes on TEER magnitudes compare to that from the 5kHz sinusoidal stimulus. If the sinusoidal stimulus frequency is decreased, then the effect of the double layer capacitance is more pronounced, making the TEER value increase as the input frequency decreases. Fig. 3e confirms this by showing the percent difference between the sinusoidal and square wave increases as the frequency of the sinusoidal stimulus decreases. When the stimulus frequency reaches 3kHz and above, the difference between sinusoidal and square wave data flattens out, indicating that the stimulus frequency is now high enough to bypass the double layer capacitance.
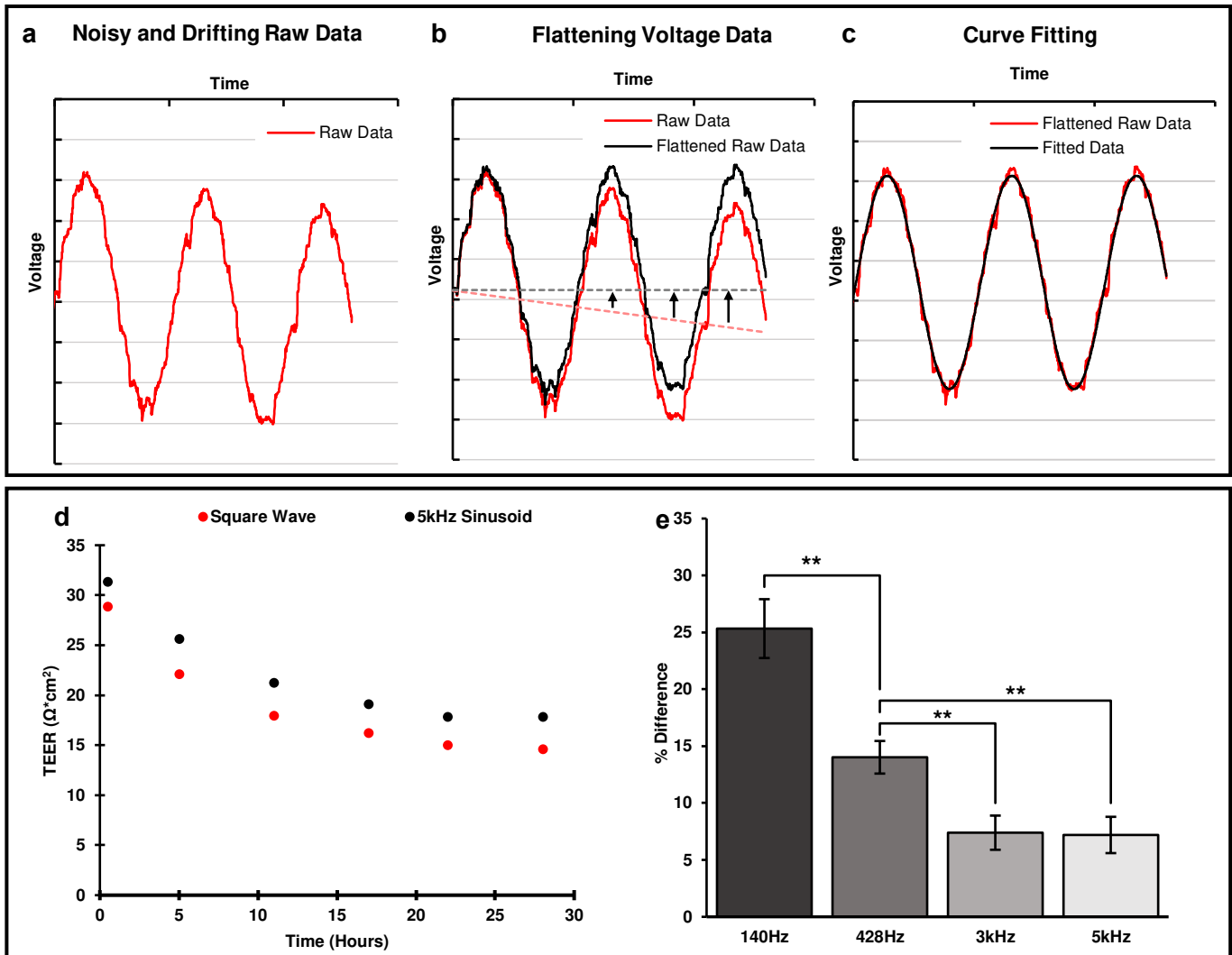
Figure 3: Response signal conditioning and the effect of stimulus signal on TEER calculation. **a)** Raw response signal with unwanted artifacts. The raw data is noisy and also drifting over time because of the offset DC from the HCS. The curve-fitted signal (black) removes the unwanted artifacts from the acquired response signal (red). **b)** An example illustrating the drift correction performed by the fitting algorithm. The 1st degree polynomial (dotted red) of the input data is subtracted point by point from the input raw data (solid red), effectively flattening it out. Once the input data is flattened out it can be fit to a sinusoidal curve (black). **c)** Curve fitting algorithm applied to flattened raw data (red) to produce noise-free fitted signal (black). **d)** Comparison of TEER measured with square wave and 5kHz sinusoidal stimulus signals. The square wave stimulus is consistently lower than the sinusoidal value. **e)** The average difference of TEER between sinusoidal and square waveforms for different frequencies of the sinusoidal waveforms, n = 10, **: P < 0.005.

Experiment and Measurement Procedure

After all tissue explants were cut and prepared according to the protocol in Section *Animals, Tissue Collection, and Media Preparation*, the explants were loaded into the microfluidic chamber, one by one. First, the explants were placed on the bottom half chamber and then gently flattened out using forceps, careful not to touch the luminal side and damage the mucosa. After the tissue was flattened and centered over the holding cavity (Fig. 1c) on the bottom half chamber, the top chamber was slid down the metal screw guides to secure the tissue in place and create a tight seal. The chamber was then tightened using wing nuts and inserted into the card edge connector on the metal enclosure of the system (Fig. 1g). Next the inlet and outlet tubing were connected. The media outlet tubes fed into empty glass bottles as a way to determine whether even media outlet from each side of the tissue was achieved during experiments. To remove any air bubbles in the chamber the media was purged into the chamber at an increased rate

(25,000 µL hr^{-1}) for 45 seconds at the start of each experiment. After the initial purge, the media flow rate was reduced to 250 µL hr^{-1} throughout the experiment. The chambers, media, and the system enclosure are all kept in an incubator set to 37 °C.

Live tissue experiments ranged from 24 h – 72 h, and a TEER measurement was performed every 2 hours. This created a timeline of the tissues' TEER values to examine the TEER changes as a function of time. For each TEER measurement the input AC current magnitude was set at 85 µA and the frequency was swept from 12Hz to 5kHz at 20 different frequency points. At each measurement point, the TEER was measured using the sinusoidal waveform stimulus as well as the square waveform stimulus.

After the experiment was completed, the chambers were disconnected from all tubing and disconnected from card edge connector. The chamber was then opened to expose the tissue sample and the tissue was preserved following the steps outlined in Section *Tissue Sectioning and Histochemistry.*

3 Results and Discussion

Results of System Electrical and Noise Performance

The frequency response of each circuit component along the signal path is shown in Figs. 4a-d. The component with the lowest bandwidth of 47.5 kHz is the TIA (Fig. 4d). The bandwidth of the TIA was set by a compensation capacitor to be roughly ten times higher than the highest frequency of input sinusoidal stimulus (5kHz). This to not attenuate any important read channel signals while also filtering out as much high frequency noise as possible. It should be noted that the TIA tends to have high input inferred noise due to the high thermal noise of its gain-setting resistors. It also sits relatively late in the analog signal chain and its low bandwidth can filter out the output noise from other components (input level shifter and HCS) before it in the signal chain. This sets the full systems bandwidth at 47.5 kHz as intended.

The stability of each read channel is examined by its step response to obtain sufficiently damped responses (Fig. 4f). The noise power spectral density (PSD) of the read channel was measured and shown in Fig. 4e. The results show the total noise power to be 0.126 µV^2, well below the minimum output signal power of 82.1 µV^2 of the system, resulting in a signal-to-noise ratio (SNR) of 28.14 dB. Other system performance parameters, such as power consumption, TEER measurement error, and the acceptable TEER range with error less than 5%, were also measured and calculated. Table 1 summarizes the system level electrical performance of the microphysiological system.
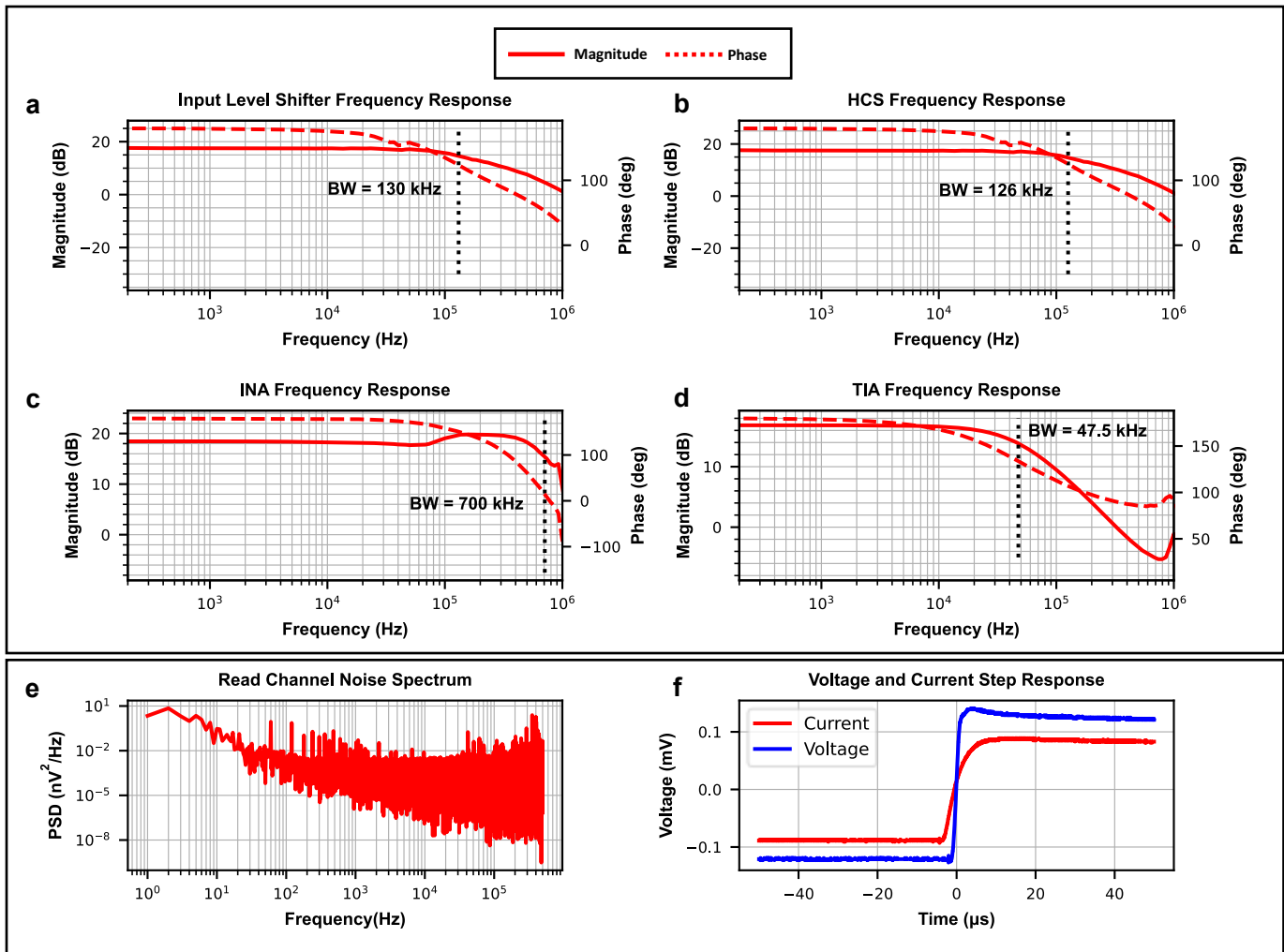
Figure 4: System electrical performance. The frequency response for each component in the signal path **(a-d)** was used to find the systems bandwidth. **a)** Input level shifter frequency response. **b)** HCS frequency response. **c)** INA frequency response. **d)** TIA frequency response. The limiting component is the TIA **(d)**, this component sets the systems bandwidth at 47.5kHz. **e)** The read channel noise power spectral density (PSD) was found to classify the noise specification of the system. **f)** The step response of the voltage and current stages in the read channel. The lack of ringing in both step responses confirm the stability of the read channel.

Tissue Viability

Tissue health was maintained in the device with barrier integrity over 72 h. Colon explants maintained proper arrangement of mucosal, submucosal, muscular layers, and patterned crypts (Fig 5a(i)). To protect the body from potential pathogens, healthy intestinal tissue must maintain sophisticated epithelial and mucosal barriers. Specialized epithelial cells, known as goblet cells, are crucial to barrier maintenance as they are responsible for producing and secreting mucin. Goblet cells were characterized due to their essential roles in maintenance of the barrier. Goblet cell mucopolysaccharides were identified by binding *Ulex europaeus* agglutinin I (UEA-1) conjugated to rhodamine. After 72 h in the microphysiological system, goblet cells retained their distinct shape (Fig 5a(ii), arrows) and the inner mucus layer remained intact confirming maintenance of the mucosal barrier (Fig 5a(ii)). To further verify barrier integrity, tight junctions were examined. Tight junctions adhere epithelial cells together forming a physical barrier between cells to prevent unwanted passage of ions and molecules between epithelial cells. Claudins are a specific type of tight junction protein that help form the backbone of tight junctions. Claudin-1 is widely expressed in the intestinal epithelium and has essential roles in tight junction integrity. After 72 h in the device, clear

claudin-1 immunoreactivity remained around epithelial cells (Fig. 5a(iii)) further indicating maintenance of tissue health and barrier integrity.

Using TEER to measure changes in barrier permeability

Changes in TEER were correlated with physiological signs of barrier impairment, such as alterations to epithelial cells, the mucus layer, and tight junction proteins. To induce a disruption to barrier permeability, the luminal side of colon tissue was treated with collagenase or acidic media. Bacterial collagenases are enzymes secreted by endogenous bacteria in the intestines that degrade collagen. Increased collagenase can break down tight junctions between epithelial cells, as well as, break down the extracellular matrix of epithelial cells[32]. This leads to increased intestinal permeability, and provides a model for the development of leaky gut syndrome[33]. We have previously shown that bacterial collagenase in luminal media can be used as a model to create leaky gut by disrupting epithelial cell (goblet cell) morphology and decreasing tight junction (claudin-1) expression[11]. Increased barrier permeability was shown by an increased reduction in TEER with collagenase treatment over time (Fig. 5b(v)). To confirm that reductions in TEER correlated with physiological characteristics of increased intestinal permeability, goblet cells and claudin-1 were examined. Following collagenase treatment, goblet cells became more circular in shape (Fig. 5b(i)) and claudin-1 immunoreactivity was moderately decreased (Fig. 5b(iii)) indicating barrier impairment.
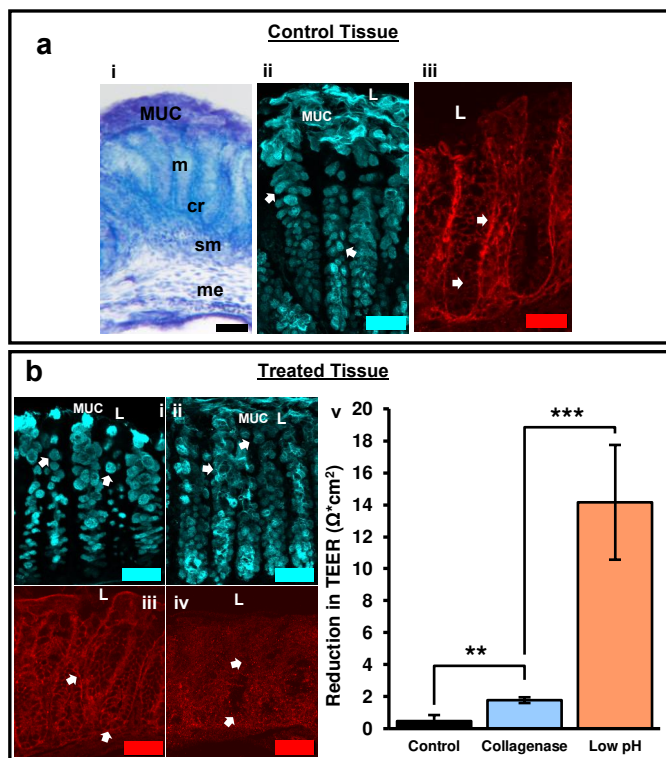

Figure 5: **Tissue health was maintained over 72 h in the device and monitored after media treatment. a)** Control tissue after 72 h experiment. i) Tol blue staining showing maintenance of colon morphology. ii) UEA-1+ material confirming maintenance of epithelial cells and mucus layer. iii) Claudin-1 immunoreactivity shows maintenance of tight junctions between epithelial cells and crypts indicated by claudin-1 immunoreactivity. MUC = mucus layer, m = mucosa, cr = crypt, sm = submucosa, me = muscularis externa. **b)** Collagenase treated, and acidic luminal media resulted in alterations in goblet cell morphology and tight junction expression indicative of increased barrier permeability. i) Goblet cells labeled with UEA-1 become circular after collagenase treatment. ii) Acidic media resulted in loss of goblet cell shape and sloughing off of cells near the lumen. iii) Alterations in tight junction protein expression (claudin-1) following collagenase treatment. iv) Claudin-1 expression decreased considerably with exposure to acidic media indicative of substantial barrier disruption. v) The bar graph shows a distinct reduction in TEER after exposure to different media composition. The difference in TEER was measured from 24 to 48-hour mark after the tissue was enclosed in the device, with the media change occurring at 24 hours. The three media compositions consist of a control media, collagenase treated media, and low pH media (more details about media composition in *"Animals, Tissue Collection, and Media Preparation"*). L = lumen, scale bars = 50μm, TEER values are normalized to the membrane surface area of the chamber, $0.0314cm^2$. Control: n = 4, Collagenase: n = 10, Low pH: n = 3, **: p < 0.005; ***: p < 0.0001

To test whether changes in TEER matched changes in physiological changes, acidic media (pH 2) was added to the luminal side of tissue to induce significant damage to the intestinal barrier. Cells need to maintain a pH of 7.4 to function properly. Lowering the pH to 2.0 leads to significant epithelial cell death and alterations in cellular processes creating drastic increases in permeability. This was confirmed with goblet cells losing distinct shape and sloughing off near the lumen (Fig. 5b(ii)). Claudin-1 immunoreactivity dramatically decreased indicating substantial loss of tight junctions (Fig. 5b(iv)). These dramatic changes

in epithelial cell and claudin-1 morphology correlate with the significant reduction of TEER following acidic pH treatment (fig. 5b(v))

Differences in tissue explant detected by TEER

Cut muscle vs. muscle intact muscle

To determine whether distinct tissue components contributed differentially to TEER, the muscle layer was dissected away. Thereby removing the muscularis externa, a major subepithelial structure of the colon. TEER was measured after 24 h inside the chamber, allowing sufficient time for the tissue to equilibrate to its new environment. Removal of the muscle layer decreased TEER by about 39% (Fig. 6a). This result is consistent with previous reports that have performed experiments to study the contribution of sub epithelial resistance. The values reported have ranged from 15% to 80% of the total epithelial resistance is concentrated in the sub epithelium, depending on the location in the intestine as well as the animal[8,30,34–36]. Research using rat jejunum has shown a much larger contribution to total resistance done by the sub epithelium (78-80%)[8,34]. Whereas measurements on the ileum, colon, and rectum in both rats and mice have showed much lower contributions (15-45%)[30,35,36]. This is consistent with the results found here using mouse colon.

Confirmation of total muscle dissection was done by Toluidine blue staining, as seen in Fig. 6a(ii) when compared to tissue with the muscle intact (Fig. 6a(i)). Demonstrating the TEER calculated with the muscle dissected is an accurate representation of the epithelial resistance alone and has little to no contribution from subepithelial resistances. This demonstration is lacking from all previous research studying the contribution of subepithelial resistance by subepithelial stripping or dissection[34–36]. These images alongside the TEER measurements provide new evidence for the contribution of subepithelial resistance to total epithelial resistance.

Proximal vs. Distal Colon

Since distal colon is generally thicker than proximal colon, we investigated if these differences in tissue thickness correlated with changes in TEER. Based on the results that an intact muscle layer increased TEER (Fig. 6a), we expected TEER to be higher in distal colon. However, we observed about a 19% decrease in TEER in the distal colon compared to the proximal colon (Fig. 6b). Interestingly, this is consistent with previous reports showing higher TEER values in mouse proximal colon compared to mid or distal colon[6]. Based on the observed effect of muscle removal, we found it likely that other factors contribute to differences in TEER between proximal and distal colon. One possible factor is luminal pH. The pH of the proximal colon is typically around 5.8-6.5, while the distal colon is typically around 7-7.6[37]. Previous studies have attributed increased TEER to decreased pH in the culture media[38]. This is consistent with our observations that an empty chamber filled with acidic media (pH 2) had higher TEER than control media (pH 7.4).

Higher TEER in proximal colon may be a function of the thickness of the mucus layer. The colon houses the majority of the intestinal microbiome and, therefore, has a thick mucus layer that physically separates bacteria from underlying epithelial cells. The proximal colon has been reported to have a thicker mucus layer compared to the distal colon with increased number and size of goblet cells, as well as increased expression of mucin-2[39]. In vivo measurements of mouse colon have estimated the colon mucus layer to be ~190 μm[40]. This is significant as the total tissue thickness of mouse colon is estimated to be is around 140-300 μm[41]. The mucus layer may have a profound effect on TEER, however, studies investigating the contribution of the mucus layer on TEER are lacking. The mucus layer can be easily washed off in tissue dissection and preparation.
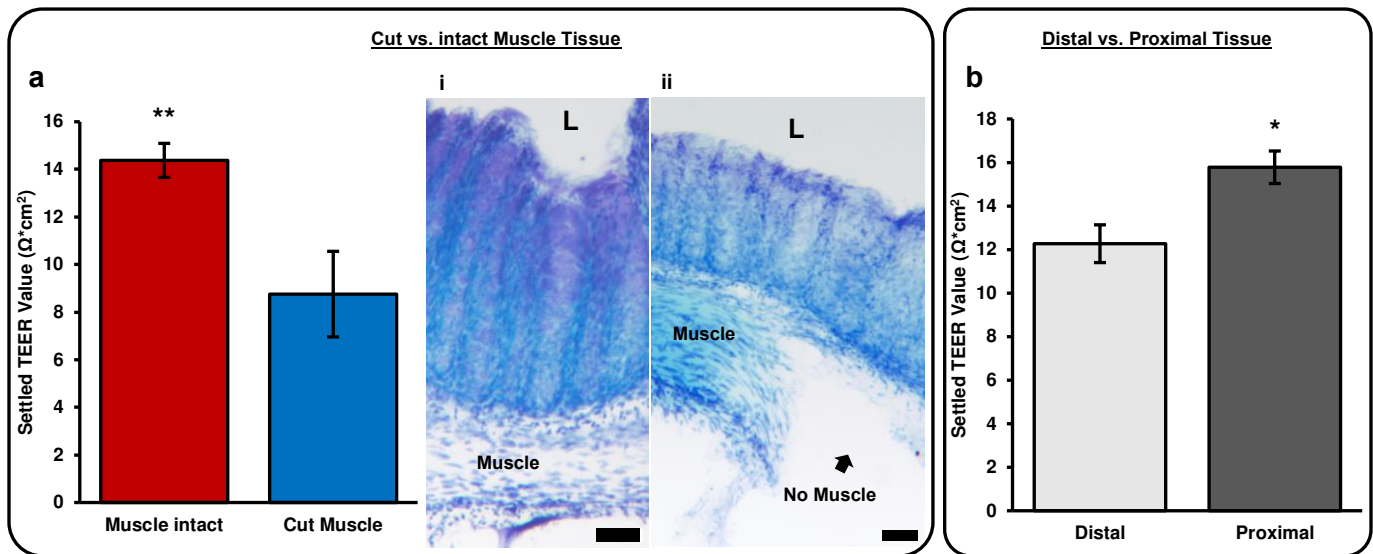
Figure 6: Physical differences in tissue explant. a) This bar chart shows the difference in settled TEER value of tissues explants with the muscle intact vs. with the muscle removed. The settled TEER value is taken 24 hours after the tissue is enclosed in the chamber. i) Tol blue staining of tissue with intact muscle. ii) Tol blue staining tissue with muscle removed, L = lumen, scale bars = 50µm. **b)** Settled TEER values for different regions of mouse colon tissue. Proximal tissue was defined as the three pieces of tissue closest to the cecum and distal tissue was defined as the two pieces farthest from the cecum and closest to the rectum. Each tissue piece was approximately 5mm in length. The settled TEER value was taken approximately 24 hours after the tissue had been enclosed in the device. Muscle intact: n = 15, Cut muscle: n = 7, Distal: n = 6, Proximal: n = 9, **: $P < 0.005$, *: $P < 0.01$.

Highlights of System Performance

Besides the electrical performance metrics and the experimental results shown above, some unique capabilities of the microphysiological system are compared with the existing systems/devices reported in the literature as illustrated in Table 2. Compared to the existing systems/devices, this system is able to maintain longer tissue viability of intestine tissue with integrated electrodes to provide real-time TEER measurements. The custom electronics and system design also provide experiment configuration and improved throughput.

4 Conclusion

This paper presents a highly integrated microphysiological system for studying live tissue barrier permeability of mouse colon. The unique design of the microfluidic chamber is capable of securing an explant of mouse colon tissue between two independent media pathways creating a micro physiological environment inside the chamber comparable to the environment in vivo. The use of proper media provides nutrients, support gut microbiome, and create important oxygen gradients across the tissue to keep tissue viability for an extended period of time. After 72 hours in the chamber, the tissue explants displayed an inner mucus layer, robust goblet cells, and evident tight junction function along the length of the epithelial layer. These characteristics all serve as strong indicators of sustained barrier integrity. This preservation of tissue viability addresses a significant drawback in existing live tissue barrier permeability devices.

Integrated electrode chips allow the microfluidic chamber to successfully characterize barrier permeability using TEER measurements in real time. The plug-and-play nature of the system design simplifies the experiment setup and allows for all chambers to be re-usable and universal. Unlike most existing systems where bulky and expensive benchtop equipment is needed to perform experiments, the integrated support electronics made the overall system small enough to fit into an incubator. Furthermore, architectural scalability allows multiple chambers to be connected to the system enabling higher throughput

of controlled experiments using samples from the same donor. The use of the system is further enhanced by a custom-built GUI which was developed to allow each experiment to be customizable and ran from any host computer.

In conclusion, this microphysiological system has the potential to open new avenues to investigate barrier health of live tissues. Real time barrier health measurements are crucial to developing more accurate ex vivo tissue models for studying the health and chemical response of epithelial cells.

Acknowledgements

References

1. Moens, E. & Veldhoen, M. Epithelial barrier biology: good fences make good neighbours. *Immunology* **135**, 1–8 (2012).

2. Walter, F. R. *et al.* A versatile lab-on-a-chip tool for modeling biological barriers. *Sensors and Actuators B: Chemical* **222**, 1209–1219 (2016).

3. Srinivasan, B. *et al.* TEER Measurement Techniques for In Vitro Barrier Model Systems. *SLAS Technology* **20**, 107–126 (2015).

4. Ussing, H. H. & Zerahn, K. Active transport of sodium as the source of electric current in the short-circuited isolated frog skin. *Acta Physiol Scand* **23**, 110–127 (1951).

5. Clarke, L. L. A guide to Ussing chamber studies of mouse intestine. *American Journal of Physiology-Gastrointestinal and Liver Physiology* **296**, G1151–G1166 (2009).

6. Thomson, A. *et al.* The Ussing chamber system for measuring intestinal permeability in health and disease. *BMC Gastroenterol* **19**, 98 (2019).

7. Poenar, D. P., Yang, G., Wan, W. K. & Feng, S. Low-Cost Method and Biochip for Measuring the Trans-Epithelial Electrical Resistance (TEER) of Esophageal Epithelium. *Materials (Basel)* **13**, 2354 (2020).

8. Fromm, M., Schulzke, J. D. & Hegel, U. Epithelial and subepithelial contributions to transmural electrical resistance of intact rat jejunum, in vitro. *Pflugers Arch* **405**, 400–402 (1985).

9. Benson, K., Cramer, S. & Galla, H.-J. Impedance-based cell monitoring: barrier properties and beyond. *Fluids and Barriers of the CNS* **10**, 5 (2013).

10. Leung, C. M. *et al.* A guide to the organ-on-a-chip. *Nat Rev Methods Primers* **2**, 1–29 (2022).

11. Cherwin, A. E. *et al.* Microfluidic organotypic device to test intestinal mucosal barrier permeability *ex vivo*. *Lab Chip* 10.1039.D3LC00615H (2023) doi:10.1039/D3LC00615H.

12. Liang, F. *et al.* A microfluidic tool for real-time impedance monitoring of in vitro renal tubular epithelial cell barrier. *Sensors and Actuators B: Chemical* **392**, 134077 (2023).

13. McLean, I. C., Schwerdtfeger, L. A., Tobet, S. A. & Henry, C. S. Powering *ex vivo* tissue models in microfluidic systems. *Lab Chip* **18**, 1399–1410 (2018).

14. Richardson, A. *et al.* A microfluidic organotypic device for culture of mammalian intestines *ex vivo*. *Anal. Methods* **12**, 297–303 (2020).

15. van der Helm, M. W. *et al.* Direct quantification of transendothelial electrical resistance in organs-on-chips. *Biosensors and Bioelectronics* **85**, 924–929 (2016).

16. Odijk, M. *et al.* Measuring direct current trans-epithelial electrical resistance in organ-on-a-chip microsystems. *Lab Chip* **15**, 745–752 (2015).

17. Yeste, J., Illa, X., Alvarez, M. & Villa, R. Engineering and monitoring cellular barrier models. *J Biol Eng* **12**, 18 (2018).

18. Thuenauer, R., Rodriguez-Boulan, E. & Römer, W. Microfluidic approaches for epithelial cell layer culture and characterisation. *Analyst* **139**, 3206–3218 (2014).

19. Helm, M. W. van der *et al.* Non-invasive sensing of transepithelial barrier function and tissue differentiation in organs-on-chips using impedance spectroscopy. *Lab Chip* **19**, 452–463 (2019).

20. Fernandes, J. *et al.* Real-time monitoring of epithelial barrier function by impedance spectroscopy in a microfluidic platform. *Lab Chip* **22**, 2041–2054 (2022).

21. Danku, A. E., Dulf, E.-H., Braicu, C., Jurj, A. & Berindan-Neagoe, I. Organ-On-A-Chip: A Survey of Technical Results and Problems. *Front Bioeng Biotechnol* **10**, 840674 (2022).

22. Ghiselli, F., Rossi, B., Piva, A. & Grilli, E. Assessing Intestinal Health. In Vitro and Ex vivo Gut Barrier Models of Farm Animals: Benefits and Limitations. *Front Vet Sci* **8**, 723387 (2021).

23. Calvo, P. C., Campo, O., Guerra, C., Castaño, S. & Fonthal, F. Design of using chamber system based on electrical impedance spectroscopy (EIS) to measure epithelial tissue. *Sensing and Bio-Sensing Research* **29**, 100357 (2020).

24. Liu, J. *et al.* The differential Howland current source with high signal to noise ratio for bioimpedance measurement system. *Rev Sci Instrum* **85**, 055111 (2014).

25. Obeidat, Y. M. *et al.* Design of a multi-sensor platform for integrating extracellular acidification rate with multi-metabolite flux measurement for small biological samples. *Biosensors and Bioelectronics* **133**, 39–47 (2019).

26. Wegener, J., Hakvoort, A. & Galla, H.-J. Barrier function of porcine choroid plexus epithelial cells is modulated by cAMP-dependent pathways in vitro. *Brain Research* **853**, 115–124 (2000).

27. Wegener, J., Abrams, D., Willenbrink, W., Galla, H.-J. & Janshoff, A. Automated multi-well device to measure transepithelial electrical resistances under physiological conditions. *Biotechniques* **37**, 590, 592–594, 596–597 (2004).

28. Gijzen, L. *et al.* An Intestine-on-a-Chip Model of Plug-and-Play Modularity to Study Inflammatory Processes. *SLAS Technol* **25**, 585–597 (2020).

29. Douville, N. J. *et al.* Fabrication of two-layered channel system with embedded electrodes to measure resistance across epithelial and endothelial barriers. *Anal Chem* **82**, 2505–2511 (2010).

30. Gitter, A. H., Fromm, M. & Schulzke, J.-D. Impedance analysis for the determination of epithelial and subepithelial resistance in intestinal tissues. *Journal of Biochemical and Biophysical Methods* **37**, 35–46 (1998).

31. Gitter, A. H., Schulzke, J.-D., Sorgenfrei, D. & Fromm, M. Ussing chamber for high-frequency transmural impedance analysis of epithelial tissues. *Journal of Biochemical and Biophysical Methods* **35**, 81–88 (1997).

32. Duarte, A. S., Correia, A. & Esteves, A. C. Bacterial collagenases - A review. *Crit Rev Microbiol* **42**, 106–126 (2016).

33. Aleman, R. S., Moncada, M. & Aryana, K. J. Leaky Gut and the Ingredients That Help Treat It: A Review. *Molecules* **28**, 619 (2023).

34. Hemlin, M., Jodal, M., Lundgren, O., Sjövall, H. & Stage, L. The importance of the subepithelial resistance for the electrical properties of the rat jejunum *in vitro*. *Acta Physiologica Scandinavica* **134**, 79–88 (1988).

35. Tai, Y.-H. & Tai, C.-Y. The conventional short-circuiting technique under-short-circuits most epithelia. *J. Membrain Biol.* **59**, 173–177 (1981).

36. Gitter, A. H., Bendfeldt, K., Schulzke, J. D. & Fromm, M. Trans/paracellular, surface/crypt, and epithelial/subepithelial resistances of mammalian colonic epithelia. *Pflugers Arch - Eur J Physiol* **439**, 477–482 (2000).

37. Mikolajczyk, A. E., Watson, S., Surma, B. L. & Rubin, D. T. Assessment of Tandem Measurements of pH and Total Gut Transit Time in Healthy Volunteers. *Clinical and Translational Gastroenterology* **6**, e100 (2015).

38. Helms, H. C., Waagepetersen, H. S., Nielsen, C. U. & Brodin, B. Paracellular tightness and claudin-5 expression is increased in the BCEC/astrocyte blood-brain barrier model by increasing media buffer capacity during growth. *AAPS J* **12**, 759–770 (2010).

39. Bergstrom, K. *et al.* Proximal colon–derived O-glycosylated mucus encapsulates and modulates the microbiota. *Science* **370**, 467–472 (2020).

40. Hugenholtz, F. & De Vos, W. M. Mouse models for human intestinal microbiota research: a critical evaluation. *Cell. Mol. Life Sci.* **75**, 149–160 (2018).

41. Abdelrahman, M. A. *et al.* High-Frequency Ultrasound for In Vivo Measurement of Colon Wall Thickness in Mice. *Ultrasound in Medicine & Biology* **38**, 432–442 (2012).

42. Leonard, F., Collnot, E.-M. & Lehr, C.-M. A three-dimensional coculture of enterocytes, monocytes and dendritic cells to model inflamed intestinal mucosa in vitro. *Mol Pharm* **7**, 2103–2119 (2010).

43. Dawson, A. *et al.* A microfluidic chip based model for the study of full thickness human intestinal tissue using dual flow. *Biomicrofluidics* **10**, 064101 (2016).

44. Eslami Amirabadi, H. *et al.* Intestinal explant barrier chip: long-term intestinal absorption screening in a novel microphysiological system using tissue explants. *Lab Chip* **22**, 326–342 (2022).

Tables

Specification	Value	Unit
Impedance Calculation		
Frequency Range	10-5k	Hz
Impedance Range (Error <5%)	150-6.5k	Ω
Sampling		
ADC Sampling Rate	806.4k	samples/s
Resolution	12	bits
Power Consumption		
V_{dd}	±5	V
Full system	4.203	W
TEER Circuit Add on	1.17	W
Signal Processing		
Bandwidth	47.5	kHz
Howland Offset Current (DC)	1.87	μA
Voltage Gain	9.8214	gain
Current Gain	27,000	gain
Noise		
SNR	28.14	dB
Total Noise Power	0.1261	μV^2
Avg. Spectral Density	623.824	$nV/\sqrt{Hz}$
Spot Noise @ 100Hz	1685.79	$nV/\sqrt{Hz}$
Spot Noise @ 1kHz	630.688	$nV/\sqrt{Hz}$
Spot Noise @ 10kHz	762.691	$nV/\sqrt{Hz}$

Table 1: Full System Specifications

	Biological Sample		Electrical Permeability				Chamber/System Design	
	Sample Type	Demonstrated Tissue Viability	TEER capable?	Electrode Type	Stimulus Signal	Measurement Electronics	Microfluidics Support	Throughput
Transswell[2,42]	Cell monolayer	-	Yes	Ag/AgCl "stick" electrodes	DC	Commercial Benchtop	No	96
Liang et al., 2023[12]	Cell monolayer (canine kidney)	-	Yes	Integrated glass chip	Up to 10MHz	Commercial Benchtop	Yes	1
Helm et al., 2019[19]	Cell monolayer (Caco-2)	-	Yes	Polycarbonate substrate electrode chips	Up to 100kHz	Commercial Benchtop	Yes	1
Fernandes et al., 2022[20]	Cell monolayer (GI tract and airway)	-	Yes	Integrated glass chip	Up to 100kHz	Custom-built	One side only	8
Navicyte[6]	Mouse and human intestinal tissue	<3 h	Yes	Ag/AgCl "stick" electrodes	DC	Commercial Benchtop	No	6
Clarke et al., 2009[5]	Mouse colon tissue	3 h	Yes	Ag/AgCl electrodes connected by salt bridge	DC	Commercial Benchtop	No	1
Calvo et al., 2020[23]	Frog epithelial tissue	-	Yes	Integrated "stick" electrodes	Up to 100kHz	Custom-built	No	1
Dawson et al., 2016[43]	Human intestine tissue	72 h	No	-	-	-	Yes	1
Poenar et al., 2020[7]	Porcine esophageal tissue	48	Yes	Integrated "stick" electrodes	DC	Commercial Benchtop	Yes	1
Cherwin et al., 2023[11] **& Richardson et al., 2020**[14]	Mouse colon tissue	72 h	No	-	-	-	Yes	1
Amirabadi et al., 2022[44]	Porcine & human colon tissue	24 h	No	Optical Fiber Sensor	-	-	Yes	1
This Work	Mouse colon tissue	72 h	Yes	Integrated glass chip	Up to 5kHz	Custom-built	Yes	3

Table 2: Comparison of epithelial barrier investigation devices